Pattern Recognition Letters 32 (2011) 694–700

Contents lists available at ScienceDirect

Pattern Recognition Letters

journal homepage: www.elsevier.com/locate/patrec

Efficient template matching for multi-channel images

Stefano Mattoccia, Federico Tombari *, Luigi Di Stefano

Department of Electronics Computer Science and Systems (DEIS), University of Bologna, Viale Risorgimento 2, 40136 Bologna, Italy
Advanced Research Center on Electronic Systems for Information and Communication Technologies (ARCES), University of Bologna, Via Toffano 2/2, 40135 Bologna, Italy

ARTICLE INFO

Article history:
Received 17 March 2010
Available online 15 December 2010
Communicated by F.Y. Shih

Keywords:
Template matching
Multi-channel images
ZNCC

ABSTRACT

Template matching is a computationally intensive problem aimed at locating a template within a image. When dealing with images having more than one channel, the computational burden becomes even more dramatic. For this reason, in this paper we investigate on a methodology to speed-up template matching on multi-channel images without deteriorating the outcome of the search. In particular, we propose a fast, exhaustive technique based on the Zero-mean Normalized Cross-Correlation (ZNCC) inspired from previous work related to grayscale images. Experimental testing performed over thousands of template matching instances demonstrates the efficiency of our proposal.

1. Introduction

Template matching (Zitová and Flusser, 2003; Goshtasby, 2005) is a computationally intensive problem that aims at locating a template T within an image I. The basic approach, or Full-Search (FS), simply computes a similarity measure between T and each possible portion of the image, referred to as the *image subwindow* or *candidate*, of the same size as T. Then, the candidate reporting the highest similarity locates the position of the template in the image.

While numerous exhaustive techniques have been recently proposed to speed-up this task based on grayscale (i.e. single-channel) images (Mattoccia et al., 2008a,b; Tombari et al., 2009; Wei and Lai, 2007; Mahmood and Khan, 2007a,b; Pan and Wei, 2008; Alkhansari, 2001), to the best of our knowledge the problem of performing fast exhaustive template matching with multi-channel images has not been addressed yet. Today, multi-channel images are used in an increasing number of computer vision tasks. Two typical examples are represented by color images and multi-spectral images: the former are commonly deployed for tasks such as defect detection and industrial quality control (e.g. Tsai et al., 2003), the latter for tasks such as medical image registration and remote sensing data alignment (Guo et al., 2009; Kern and Pattichis, 2007; Pope and Theiler, 2003).

In this paper we propose a fast template matching technique for multi-channel images based on the Zero-mean Normalized Cross-Correlation (ZNCC), a measure which is widely used for grayscale template matching (Mattoccia et al., 2008b; Mahmood and Khan, 2007a,b). The proposed technique is exhaustive, i.e. it guarantees to find always the global maximum of the correlation function, and it is inspired by the ZEBC technique (Mattoccia et al., 2008b), previously proposed for grayscale images. The basic idea is to find efficiently computable upper bounding functions of the ZNCC that allow rapid detection of mismatching candidates.

The paper is structured as follows. Section 2 introduces the notation and the definitions used throughout the paper. Then, Sections 3 and 4 describe the mathematical grounds and the proposed algorithm. Section 5 shows experimental results on a vast dataset composed of color images. Finally, conclusions are drawn in Section 6.

2. Notation

Let T and $I(x,y)$ be respectively a template and an image subwindow with C channels, the template size being $M \times N$:

$$T = [T_1, \ldots, T_k, \ldots, T_c]^T. \tag{1}$$

$$I(x,y) = [I_1(x,y), \ldots, I_k(x,y) \ldots, I_c(x,y)]^T, \tag{2}$$

where

$$T_k = [T_k(1,1), \ldots, T_k(M,N)]^T, \tag{3}$$

$$I_k(x,y) = [I_k(x+1,y+1), \ldots, I_k(x+N,y+M)]^T. \tag{4}$$

The ZNCC on multi-channel images can be defined as follows:

$$\zeta(x,y) \triangleq \frac{\sum_{k=1}^{C}(I_k(x,y) - \mu_I(x,y)) \circ (T_k - \mu_T)}{\sqrt{\sum_{k=1}^{C}\|I_k(x,y) - \mu_I(x,y))\|_2^2} \cdot \sqrt{\sum_{k=1}^{C}\|T_k - \mu_T\|_2^2}} \tag{5}$$

with $\circ$ denoting the dot product between two $M \times N$ vectors, and μ_T, $\mu_I(x,y)$ the mean values of respectively the template and the image subwindow:

* Corresponding author at: Department of Electronics Computer Science and Systems (DEIS), University of Bologna, Viale Risorgimento 2, 40136 Bologna, Italy. Tel.: +39 0512093545; fax: +39 0512093073.
E-mail address: federico.tombari@unibo.it (F. Tombari).

0167-8655/$ - see front matter © 2010 Elsevier B.V. All rights reserved.
doi:10.1016/j.patrec.2010.12.004

$$\mu_T \triangleq \frac{1}{C \cdot M \cdot N} \sum_{k=1}^{C} \sum_{j=1}^{N} \sum_{i=1}^{M} T_k(i,j), \tag{6}$$

$$\mu_I(x,y) \triangleq \frac{1}{C \cdot M \cdot N} \sum_{k=1}^{C} \sum_{j=1}^{N} \sum_{i=1}^{M} I_k(x+i,y+j). \tag{7}$$

The numerator in (5), here referred to as $\psi_{ZC}(x,y)$, can be seen as the sum of C different terms, associated with each of the channels of I and T:

$$\psi_{ZC}(x,y) = \sum_{k=1}^{C} \psi_{Z_k}(x,y), \tag{8}$$

where $\psi_{Z_k}(x,y)$ can be expressed as:

$$\psi_{Z_k}(x,y) \triangleq \sum_{j=1}^{N} \sum_{i=1}^{M} (I_k(x+i,y+j) - \mu_I(x,y)) \cdot (T_k(i,j) - \mu_T). \tag{9}$$

We point out that another possible definition of the multi-channel ZNCC (Tsai et al., 2003), derived as an extension from its "single-channel" version, would subtract to each component of T, I in (5) the corresponding mean value computed only on that specific channel. Though not reported here for the sake of brevity, our experimental analysis has highlighted that these two definitions lead to similar performance of the ZNCC function and that the efficiency of the proposed algorithm is not affected by the use of either definition of the ZNCC. The extension of the proposed algorithm to this alternative definition of multi-channel ZNCC is anyway straightforward.

The previous expression can be algebraically manipulated to obtain:

$$\psi_{Z_k}(x,y) = \psi_k(x,y) - M \cdot N \cdot \mu_I(x,y) \cdot \mu_T \tag{10}$$

with $\psi_k(x,y)$ given by:

$$\psi_k(x,y) \triangleq \sum_{j=1}^{N} \sum_{i=1}^{M} I_k(x+i,y+j) \cdot T_k(i,j). \tag{11}$$

Hence, (5) can be rewritten as follows:

$$\zeta(x,y) = \frac{\sum_{k=1}^{C}(\psi_k(x,y)) - C \cdot M \cdot N \cdot \mu_I(x,y) \cdot \mu_T}{\sqrt{\sum_{k=1}^{C}(\|I_k(x,y)\|^2) - C \cdot M \cdot N \cdot \mu_I^2(x,y)} \cdot \sqrt{\sum_{k=1}^{C}(\|T_k\|^2) - C \cdot M \cdot N \cdot \mu_T^2}}. \tag{12}$$

Compared to (5), in this new formulation of the ZNCC function the two terms appearing at the denominator can be computed very efficiently: that concerning the template once at initialization time, the other one, concerning the image subwindow, using incremental techniques (McDonnel, 1981; Crow, 1984) in order to compute the L_2 norms and the mean value.

2.1. Partial terms

We define $\psi_{ZC}(x,y)|_\rho^\theta$ as the term representing the numerator of the ZNCC function computed between rows $(\rho,\theta)(\rho,\theta \in \{1,N\})$:

$$\psi_{ZC}(x,y)|_\rho^\theta \triangleq \sum_{k=1}^{C} \psi_{Z_k}(x,y)|_\rho^\theta \tag{13}$$

with $\psi_{Z_k}(x,y)|_\rho^\theta$ given by:

$$\psi_{Z_k}(x,y)|_\rho^\theta \triangleq \sum_{j=\rho}^{\theta} \sum_{i=1}^{M} (I_k(x+i,y+j) - \mu_I(x,y))) \cdot (T_k(i,j) - \mu_T). \tag{14}$$

We also define the generic *partial correlation* term referred to the kth channel component and computed between rows ρ and θ as:

$$\psi_k(x,y)|_\rho^\theta \triangleq \sum_{j=\theta}^{\rho} \sum_{i=1}^{M} I_k(x+i,y+j) \cdot T_k(i,j). \tag{15}$$

Analogously, we define the L_2 *partial norms* between rows ρ and θ, for the kth channel component of template and image subwindow:

$$\|T_k|\|_\rho^\theta \triangleq \sqrt{\sum_{j=\rho}^{\theta} \sum_{i=1}^{M} T_k^2(i,j)}, \tag{16}$$

$$\|I_{k_c}(x,y)|\|_\rho^\theta \triangleq \sqrt{\sum_{j=\rho}^{\theta} \sum_{i=1}^{M} I_k^2(x+i,y+j)} \tag{17}$$

and also the mean values among all channel components computed between rows ρ and θ for template and image subwindow:

$$\mu_T|_\rho^\theta \triangleq \frac{1}{C \cdot M \cdot (\theta - \rho + 1)} \cdot \sum_{k=1}^{C} \sum_{j=\rho}^{\theta} \sum_{i=1}^{M} T_k(i,j), \tag{18}$$

$$\mu_I(x,y)|_\rho^\theta \triangleq \frac{1}{C \cdot M \cdot (\theta - \rho + 1)} \cdot \sum_{k=1}^{C} \sum_{j=\rho}^{\theta} \sum_{i=1}^{M} I_k(x+i,y+j). \tag{19}$$

Finally, indicating with ξ the sum of the elements of a vector, we will refer to the *partial sum* of the kth channel component computed between rows ρ and θ for template and image subwindow as:

$$\xi(I_k(x,y))|_\rho^\theta \triangleq \sum_{j=\rho}^{\theta} \sum_{i=1}^{M} I_k(x+i,y+j) = M \cdot (\theta - \rho + 1) \cdot \mu_I(x,y))|_\rho^\theta, \tag{20}$$

$$\xi(T_k)|_\rho^\theta \triangleq \sum_{j=\rho}^{\theta} \sum_{i=1}^{M} T_k(i,j) = M \cdot (\theta - \rho + 1) \cdot \mu_T|_\rho^\theta. \tag{21}$$

3. Upper-bounding functions

Given the definition of partial correlation term $\psi_{ZC}(x,y)|_\rho^\theta$ in (13), we can determine two different upper-bounds of this term that can be usefully deployed to establish sufficient conditions aimed at efficient detection of mismatching candidates, that is, candidates that can not improve the current ZNCC maximum.

3.1. First upper-bound

By applying the Cauchy–Schwarz inequality to (13), we obtain the following upper-bound for $\psi_{ZC}(x,y)|_\rho^\theta$:

$$\beta'_{ZC}(x,y)|_\rho^\theta \triangleq \sum_{k=1}^{C} \left(\sqrt{\sum_{j=\rho}^{\theta} \sum_{i=1}^{M} (I_k(x+i,y+j) - \mu_I(x,y))^2} \cdot \sqrt{\sum_{j=\rho}^{\theta} \sum_{i=1}^{M} (T_k(i,j) - \mu_T)^2} \right). \tag{22}$$

Then, by algebraic manipulations (22) can be rewritten as:

$$\beta'_{ZC}(x,y)\big|_\rho^\theta = \sum_{k=1}^{C}\left[\sqrt{\left(\|T_k|\|_\rho^\theta\right)^2 + (\theta-\rho+1)\cdot M\cdot\mu_T^2 - 2\cdot\mu_T\cdot\xi(T_k)|_\rho^\theta}\cdot\sqrt{\left(\|I_k(x,y)|\|_\rho^\theta\right)^2 + (\theta-\rho+1)\cdot M\cdot\mu_I^2(x,y) - 2\cdot\mu_I(x,y)\cdot\xi(I_k(x,y))|_\rho^\theta}\right]. \quad (23)$$

Hence, $\beta'_{ZC}(x,y)\big|_\rho^\theta$ represents an upper-bound for the partial numerator of the ZNCC function, $\psi_{ZC}(x,y)|_\rho^\theta$:

$$\beta'_{ZC}(x,y)\big|_\rho^\theta \geqslant \psi_{ZC}(x,y)|_\rho^\theta. \quad (24)$$

3.2. Second upper-bound

By algebraic manipulations (13) can be re-written as:

$$\psi_{ZC}(x,y)|_\rho^\theta = \sum_{k=1}^{C}(\psi_k(x,y)|_\rho^\theta - \mu_T\cdot\xi(I_k(x,y))|_\rho^\theta - \mu_I(x,y)\cdot\xi(T)|_\rho^\theta + (\theta-\rho+1)\cdot M\cdot\mu_T\cdot\mu_I(x,y)). \quad (25)$$

Then, the Cauchy–Schwarz inequality can be applied to the term $\psi_k(x,y)|_\rho^\theta$ appearing in (25). This approach leads to a different upper bounding function $\beta''_{ZC}(x,y)\big|_\rho^\theta$:

$$\beta''_{ZC}(x,y)\big|_\rho^\theta \triangleq \sum_{k=1}^{C}\left(\|I_k(x,y)|\|_\rho^\theta\cdot\|T_k|\|_\rho^\theta - \mu_T\cdot\xi(I_k(x,y))|_\rho^\theta - \mu_I(x,y)\cdot\xi(T_k)|_\rho^\theta + (\theta-\rho+1)\cdot M\cdot\mu_T\cdot\mu_I(x,y)\right). \quad (26)$$

3.3. Succession of bounding function

It is now possible to determine a succession of upper-bounding functions characterized by increasing tightness to the ZNCC numerator, $\psi_{ZC}(x,y)|_\rho^\theta$, and increasing computational cost. For this goal, we define functions $\beta'_{ZC,k}(x,y)\big|_\theta^\rho$ and $\beta''_{ZC,k}(x,y)\big|_\theta^\rho$:

$$\beta'_{ZC,k}(x,y)\Big|_\rho^\theta = \sqrt{\left(\|T_k|\|_\rho^\theta\right)^2 + (\theta-\rho+1)\cdot M\cdot\mu_T^2 - 2\cdot\mu_T\cdot\xi(T_k)|_\rho^\theta}\cdot\sqrt{\left(\|I_k(x,y)|\|_\rho^\theta\right)^2 + (\theta-\rho+1)\cdot M\cdot\mu_I^2(x,y) - 2\cdot\mu_I(x,y)\cdot\xi(I_k(x,y))|_\rho^\theta}, \quad (27)$$

$$\beta''_{ZC,k}(x,y)\Big|_\rho^\theta \triangleq \|I_k(x,y)|\|_\rho^\theta\cdot\|T_k|\|_\rho^\theta - \mu_T\cdot\xi(I_k(x,y))|_\rho^\theta - \mu_I(x,y)\cdot\xi(T_k)|_\rho^\theta + (\theta-\rho+1)\cdot M\cdot\mu_T\cdot\mu_I(x,y), \quad (28)$$

which represent the kth channel components of, respectively, terms $\beta'_{ZC}(x,y)\big|_\rho^\theta$ and $\beta''_{ZC}(x,y)\big|_\rho^\theta$ in (23) and (26). Given the bounding properties of these terms, it can be easily inferred that $\beta'_{ZC,k}(x,y)\Big|_\rho^\theta$ and $\beta''_{ZC,k}(x,y)\Big|_\rho^\theta$ represent two upper-bounds of $\psi_{Z_k}(x,y)|_\rho^\theta$:

$$\beta'_{ZC,k}(x,y)\Big|_\rho^\theta \geqslant \psi_{Z_k}(x,y)|_\rho^\theta, \quad (29)$$

$$\beta''_{ZC,k}(x,y)\Big|_\rho^\theta \geqslant \psi_{Z_k}(x,y)|_\rho^\theta. \quad (30)$$

In the following, we will denote as $\beta_k^B(x,y)\big|_\rho^\theta$ the bound that, between the two, approximates $\psi_{Z_k}(x,y)|_\rho^\theta$ more closely:

$$\beta_k^B(x,y)\big|_\rho^\theta = min\left\{\beta'_{ZC,k}(x,y)\Big|_\rho^\theta, \beta''_{ZC,k}(x,y)\Big|_\rho^\theta\right\}. \quad (31)$$

Thus, $\beta_k^B(x,y)\big|_\rho^\theta$ represents, for each point, the bound that is more effective in determining if the current candidate is a mismatching one.

We can then determine an upper bound for $\psi_{ZC}(x,y)|_\rho^\theta$ by summing up all partial bound terms applied on each single channel component $\beta_k^B(x,y)\big|_\rho^\theta$:

$$\gamma_1(x,y)|_\rho^\theta \triangleq \sum_{k=1}^{C}\beta_k^B(x,y)\big|_\rho^\theta \geqslant \psi_{ZC}(x,y)|_\rho^\theta. \quad (32)$$

This upper bound is composed of terms that do not include any correlation term, but only partial means, partial sums and partial norms (see Eqs. (23), (26)). Hence, it can be computed very efficiently by means of incremental techniques (McDonnel, 1981; Crow, 1984) requiring a small and fixed number of elementary operations (e.g. 4 for McDonnel, 1981). As it will be shown in the next Section, the upper bound in (32) can be usefully employed to rapidly and safely detect mismatching candidates.

It is also important to notice that, to better approximate term $\psi_{ZC}(x,y)|_\rho^\theta$, other bounding functions can be determined by iteratively substituting to each of the k partial correlation terms $\psi_{Z_k}(x,y)|_\rho^\theta$ its corresponding partial bounding term:

$$\gamma_2(x,y)|_\rho^\theta \triangleq \psi_{Z_1}(x,y)|_\rho^\theta + \sum_{k=2}^{C}\beta_k^B(x,y)\big|_\rho^\theta \quad (33)$$

$$\cdots$$

$$\gamma_C(x,y)|_\rho^\theta \triangleq \sum_{k=1}^{C-1}\psi_{Z_k}(x,y)|_\rho^\theta + \beta_C^B(x,y)\big|_\rho^\theta, \quad (34)$$

so as to obtain the following succession of increasingly tighter bounding functions:

$$\psi_{ZC}(x,y)|_\rho^\theta \leqslant \gamma_C(x,y)|_\rho^\theta \leqslant \cdots \leqslant \gamma_2(x,y)|_\rho^\theta \leqslant \gamma_1(x,y)|_\rho^\theta. \quad (35)$$

Of course, analogous formulations can be derived by using different criteria of substitution between the various channel components. Here, in lack of more advanced criteria and with the aim of outlining a general method, we have chosen to substitute the partial correlation terms with the corresponding partial bound term simply based on the lexicographic ordering of channel components.

4. The proposed algorithm

This Section proposes a novel algorithm for fast and exhaustive template matching on multi-channel images inspired by the ZEBC approach described in (Mattoccia et al., 2008b). First of all, we partition image subwindow and template as proposed in (Mattoccia et al., 2008b), that is, we divide them into an equal number of r rectangular regions (assuming that N is a multiple of r).[1] Each region is characterized by the same width (M) and the same height ($\frac{N}{r}$).

Now, we want to apply $\gamma_1(x,y)|_\rho^\theta$ on each of the r regions determined by the adopted partitioning scheme. For the sake of clarity,

[1] Although this uniform partitioning scheme is not mandatory, we adopt it for simplicity.

Fig. 1. Some images of the dataset together with some templates randomly extracted from them.

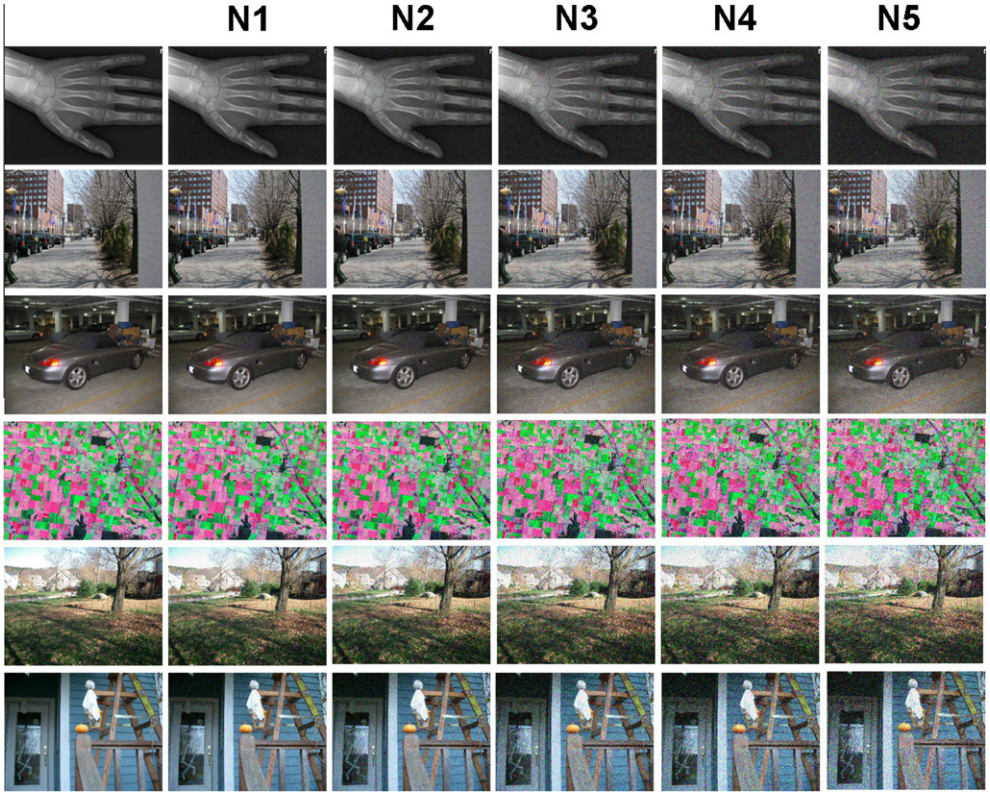

Fig. 2. Some images of the dataset and their respective versions corrupted by different Gaussian noise levels ($N1,\ldots,N5$).

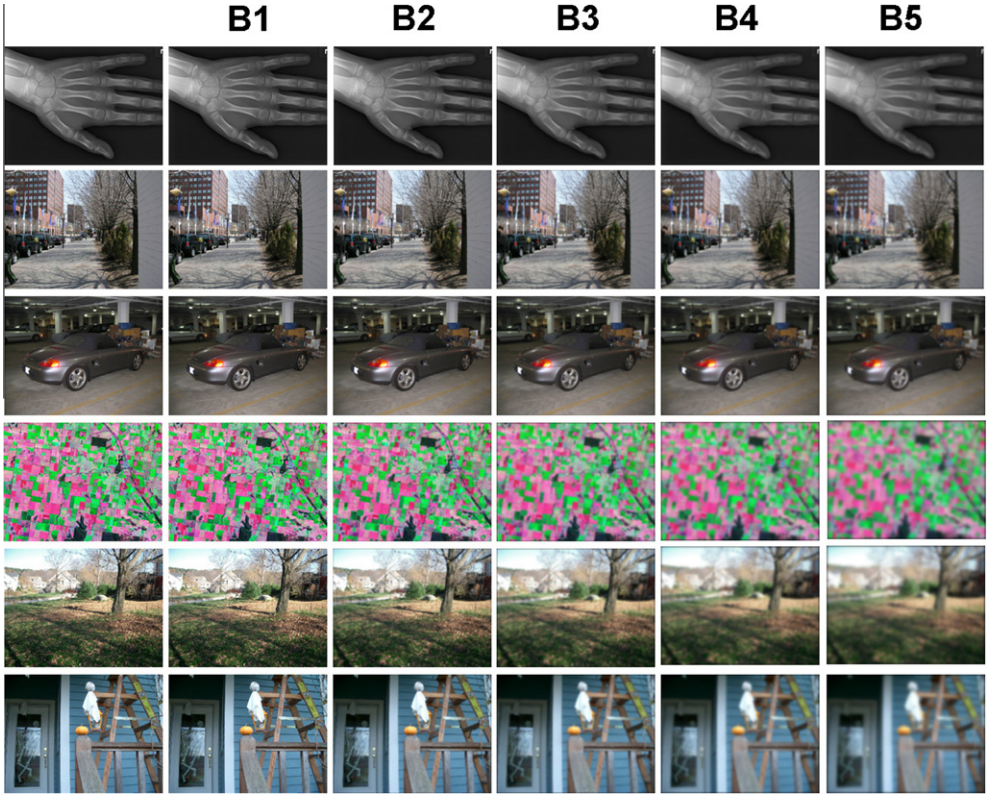

Fig. 3. Some images of the dataset and their respective versions corrupted by different blur levels ($B1,\ldots,B5$).

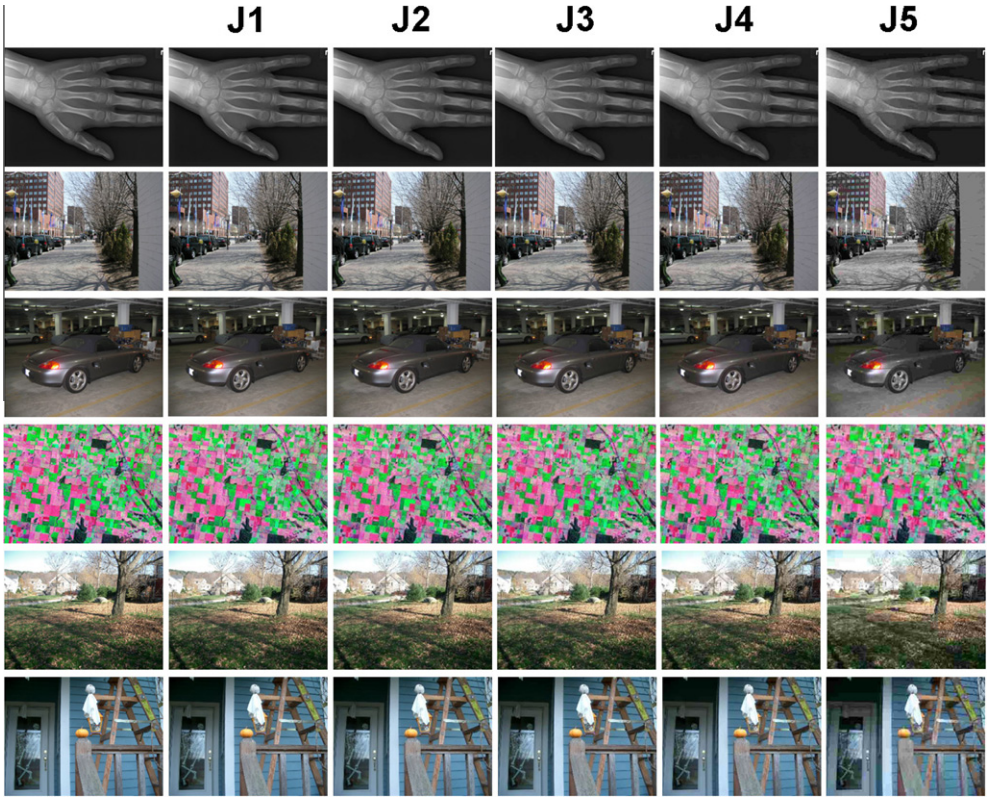

Fig. 4. Some images of the dataset and their respective versions corrupted by different JPEG compression levels ($J1,\ldots,J5$).

we will hereinafter use the pipe symbol with a single index, $|_t$, to denote the application of a term on the tth region instead than between two rows. Since each $\gamma_1(x,y)|_t$ is an upper bound of the corresponding partial numerator term $\psi_{ZC}(x,y)|_t$, and since:

$$\psi_{ZC}(x,y) = \sum_{t=1}^{r} \psi_{ZC}(x,y)\Big|_t, \tag{36}$$

then it is straightforward to derive an upper bound for term $\psi_{ZC}(x,y)$ by summing up each $\gamma_1(x,y)|_t$ computed on each region:

$$\gamma_1^1(x,y) = \sum_{t=1}^{r} \gamma_1(x,y)\Big|_t \geqslant \psi_{ZC}(x,y). \tag{37}$$

This upper bound can be deployed to determine a sufficient condition aimed at understanding if the current candidate can be a possible global maximum by means of the following relationship:
with ζ_M being the current maximum of the ZNCC function. If (38)

$$\frac{\gamma_1^1(x,y)}{\sqrt{\sum_{k=1}^{C}(\|I_k(x,y)\|^2) - C\cdot M\cdot N\cdot \mu_I^2(x,y)}\cdot\sqrt{\sum_{k=1}^{C}(\|T_k\|^2) - C\cdot M\cdot N\cdot \mu_T^2}} < \zeta_M \tag{38}$$

holds, then the candidate at position (x,y) can not be the global maximum and therefore the ZNCC term for this position does not need to be evaluated. Conversely, if (38) does not hold, a tighter bounding function can be obtained by computing the term ψ_{Z_k} on the first color component of the first region:

$$\gamma_2^1(x,y) = \gamma_2(x,y)|_1 + \sum_{t=2}^{r} \gamma_1(x,y)|_t \geqslant \psi_{ZC}(x,y). \tag{39}$$

This new bounding function can be deployed to check again whether the current candidate is a mismatching one through a sufficient condition analogous to (38). Hence, a succession of increasingly tighter upper bounding function can be determined:

$$\begin{aligned}\gamma_1^1(x,y) &\geqslant \gamma_2^1(x,y) \geqslant \cdots \geqslant \gamma_C^1(x,y) \geqslant \gamma_1^2(x,y) \geqslant \cdots \\ &\geqslant \gamma_C^2(x,y) \geqslant \cdots \geqslant \gamma_1^r(x,y) \geqslant \cdots \geqslant \gamma_C^r(x,y),\end{aligned} \tag{40}$$

where, in each term appearing in the inequalities, the superscript denotes the partition $(1,\ldots,r)$ and the subscript denotes the channel $(1,\ldots,C)$. Thus, the total number of sufficient conditions to be iteratively computed and tested is equal to $C\cdot r$. If none of these conditions holds, then the ZNCC can be computed by calculating the partial correlation term on the last channel component of the last region.

It is worth pointing out that, though not described here, this approach can be applied easily to template matching on multi-channel images based on the NCC function.

5. Experimental results

This section presents an experimental evaluation aimed at assessing the effectiveness of the proposed algorithm in speeding-up ZNCC-based template matching on multi-channel images. In particular, we tested the performance of the proposed algorithm on a dataset of color images of various contents. In particular, they were chosen from 3 different image databases: one concerning mainly indoor, urban and natural environments (MIT-CSAIL database of objects and scenes, 2005), one concerning medical images (Lukas Corpus Medical Image database, 2002) and the third concerning remote sensing imagery (NASA Landsat circa 1990/2000 coverage, 2000). The total number of images used for our evaluation is 60, composed of 30 images sized 320×240 (group $S1$) and 30 images sized 640×480 (group $S2$). All images are in RGB format (hence, $C=3$).

For each image of the dataset, 10 template coordinates were randomly extracted, only rejecting those whose standard deviation of pixel intensities did not reach a pre-defined threshold (i.e. 45). The template size was set to 32×32 for the images belonging to group $S1$ and to 64×64 for those belonging to group $S2$. Some images from the dataset together with some templates -enlarged for visualization purposes- are shown in Fig. 1.

Successively, 3 different distorted sets of the image dataset are built by adding different kinds of corruption to the original images. In particular, a first set of distorted images is built by adding to each image 5 different levels of i.i.d. zero-mean Gaussian noise, referred to as $N1,\ldots,N5$. The 5 noise levels range from very low noise to very high noise, the variances of the Gaussian distributions being respectively 1.3, 2.6, 5.1, 7.7, 10.2.[2] A subset of the dataset, including images affected by increasing levels of Gaussian noise, is shown in Fig. 2. Another set of distorted images is built by corrupting each image with 5 different blur levels obtained by Gaussian low-pass filters. The 5 blurring levels, referred to as $B1,\ldots,B5$, correspond to Gaussian filters having standard deviation $\sigma = 0.2$, 0.9, 1.6, 2.3 and 3 respectively. A subset of the dataset, including images affected by increasing levels of blur, is shown in Fig. 3. A final set of distorted images is obtained by adding to each image 5 different levels of JPEG compression, referred to as $J1,\ldots,J5$ and corresponding to quality measures $Q_{JPG} = 90$, 70, 50, 30 and 10 respectively (higher Q_{JPG} meaning lower image degradation due to compression). A subset of the dataset, including images affected by increasing levels of JPEG compression, is shown in Fig. 4.

Then, each template is matched against all corrupted versions of the corresponding image, yielding an overall number of 9000 template matching instances on which the proposed algorithm was tested.

The results of the proposed experimental evaluation are shown in Tables 1–3, corresponding, respectively, to the case of images corrupted by Gaussian noise, blur and JPEG compression. Each table reports, for the different levels of corruption, for both image sizes ($S1$,$S2$), and for different values of parameter r ($r = 2,4,8$) the mean speed-ups, measured as ratios of execution times, yielded by the proposed algorithm with respect to the FS algorithm. More specifically, each mean speed-up is obtained by averaging single speed-ups over 300 template matching instances (10 templates for 30 images). Moreover, the table reports the standard deviation associated to each mean speed-up value.

As it can be seen from the Tables, the proposed algorithm is substantially faster than the FS algorithm. As one could have expected, the computational benefits decrease with higher corruption levels, since the bounding functions approximate better the numerator of the ZNCC with less presence of corruption. It is also worth pointing out that the proposed algorithm is always faster than the FS with both image sizes used, and it seems to perform better with bigger images, probably due to the fact that with smaller images the computational overhead associated with those terms included in the ZNCC function (12) that do not concern correlation is more

[2] Corresponding to 0.005, 0.01, 0.02, 0.03, 0.04 on normalized pixel intensities ranging within [0,1].

Table 1
Speed-ups yielded by the proposed technique vs. FS on the dataset corrupted by different levels of Gaussian noise ($N1,\ldots,N5$).

	S1						S2					
r	2		4		8		2		4		8	
	μ	σ	μ	σ	μ	σ	μ	σ	μ	σ	μ	σ
N1	4.1	2.0	3.8	1.2	2.6	0.6	8.4	5.5	11.1	3.3	8.3	1.2
N2	3.2	1.7	3.3	1.2	2.4	0.7	5.7	4.0	8.3	3.6	7.0	1.9
N3	2.4	1.5	2.5	1.1	2.0	0.7	3.6	2.8	5.2	3.1	4.9	2.1
N4	2.0	1.4	2.1	1.0	1.7	0.6	2.6	2.1	3.7	2.5	3.7	2.0
N5	1.7	1.3	1.8	1.0	1.5	0.6	2.1	1.7	2.9	2.1	2.9	1.7

Table 2
Speed-ups yielded by the proposed technique vs. FS on the dataset corrupted by different levels of blur ($B1,\ldots,B5$).

	S1						S2					
r	2		4		8		2		4		8	
	μ	σ	μ	σ	μ	σ	μ	σ	μ	σ	μ	σ
B1	7.0	2.6	4.3	1.3	2.7	0.7	24.9	5.9	14.7	2.9	8.9	1.5
B2	4.1	2.0	3.8	1.1	2.6	0.5	12.0	8.0	12.0	4.4	8.2	2.0
B3	3.1	1.7	3.1	1.3	2.3	0.7	8.6	6.6	10.0	5.0	7.4	2.5
B4	2.6	1.6	2.7	1.2	2.1	0.7	7.0	5.8	8.8	5.0	6.7	2.8
B5	2.2	1.4	2.4	1.2	1.9	0.7	6.0	5.1	7.9	4.9	6.3	2.9

Table 3
Speed-ups yielded by the proposed technique vs. FS on the dataset corrupted by different levels of JPEG compression ($J1,\ldots,J5$).

	S1						S2					
r	2		4		8		2		4		8	
	μ	σ	μ	σ	μ	σ	μ	σ	μ	σ	μ	σ
J1	6.2	2.5	4.3	1.4	2.7	0.7	20.4	7.3	14.5	3.1	8.9	1.6
J2	5.3	2.4	4.2	1.4	2.7	0.7	16.1	8.0	13.9	3.4	8.8	1.5
J3	4.8	2.4	4.1	1.4	2.6	0.7	13.8	7.9	13.1	3.7	8.6	1.7
J4	4.3	2.3	3.9	1.4	2.6	0.7	12.1	7.7	12.4	4.0	8.4	1.8
J5	3.5	2.0	3.5	1.3	2.4	0.7	8.5	6.5	10.2	4.6	7.5	2.3

prominent. Finally, overall the best value of parameter r seems to be $r = 4$ for images corrupted by Gaussian noise, and $r = 2$ for images corrupted by blur and JPEG compression.

6. Conclusions

We have presented an approach that performs fast exhaustive template matching with multi-channel images based on the ZNCC function. The proposed method generalizes the ZEBC technique (Mattoccia et al., 2008b) to the case of images with a generic number of channels. Moreover, though not shown here for the sake of brevity, the proposed method can be easily adapted to work with the NCC function. Experimental results have demonstrated the effectiveness of the proposed bounding functions to rapidly detect mismatching candidates, yielding notable speed-ups with respect to the FS algorithm.

References

Alkhansari, M., 2001. A fast globally optimal algorithm for template matching using low-resolution pruning. IEEE Trans. Image Process. 10 (4), 526–533.

Crow, F., 1984. Summed-area tables for texture mapping. Comput. Graphics 18 (3), 207–212.

Lukas Corpus Medical Image database, 2002. <www.data-ompression.info/Corpora/LukasCorpus>.

Goshtasby, A., 2005. 2D and 3D Image Registration for Medical Remote, Sensing and Industrial Applications. Wiley.

Guo, J., Sun, H., Zhu, C., Xiao, S., 2009. Multispectral remote sensing image registration based on maximally stable extremal regions. In: Proceedings of SPIE Multispectral Image Acquisition and Processing (MIPPR). pp. 749412–749416.

Kern, J., Pattichis, M., 2007. Robust multispectral image registration using mutual-information models. IEEE Trans. Geosci. Remote Sens. 45 (5), 1494–1505.

Mahmood, A., Khan, S., 2007a. Early termination algorithms for correlation coefficient based block matching. In: Proceedings of International Conference on Image Processing (ICIP 07). vol. 2. pp. 469–472.

Mahmood, A., Khan, S., 2007b. Exploiting inter-frame correlation for fast video to reference image alignment. In: Proceedings of Asian Conference on Computer Vision (ACCV 07). pp. 647–656.

Mattoccia, S., Tombari, F., Di Stefano, L., 2008a. Fast full-search equivalent template matching by enhanced bounded correlation. IEEE Trans. Image Process. 17 (4), 528–538.

Mattoccia, S., Tombari, F., Di Stefano, L., 2008b. Reliable rejection of mismatching candidates for efficient ZNCC template matching. In: Proceedings of IEEE International Conference on Image Processing (ICIP 2008). pp. 849–852.

Mc Donnel, M., 1981. Box-filtering techniques. Comput. Graphics Image Process. 17, 65–70.

MIT-CSAIL database of objects and scenes, 2005. <http://people.csail.mit.edu/torralba/images>.

NASA Landsat circa 1990/2000 coverage, 2000. <http://zulu.ssc.nasa.gov/mrsid>.

Pan, W., Wei, S., 2008. Efficient ncc-based image matching in walsh-hadamard domain. In: Proceedings of 10th European Conference on Computer Vision (ECCV 08). pp. 468–480.

Pope, P., Theiler, J., 2003. Automated image registration (air) of mti imagery. In: Proceedings of SPIE 5093, 294305.

Tombari, F., Mattoccia, S., Di Stefano, L., 2009. Full search-equivalent pattern matching with incremental dissimilarity approximations. IEEE Trans. Pattern Anal. Machine Intell. (PAMI) 31 (1), 129–141.

Tsai, D., Lin, C., Chen, J., 2003. The evaluation of normalized cross correlations for defect detection. Pattern Recognit. Lett. 24, 2525–2535.

Wei, S., Lai, S., 2007. Efficient normalized cross correlation based on adaptive multilevel successive elimination. In: Proceedings of Asian Conference on Computer Vision (ACCV 07).

Zitová, B., Flusser, J., 2003. Image registration methods: A survey. Image Vision Comput. 21 (11), 977–1000.